Electronic Supplementary Information

Increased Activity in Hydrogen Evolution Electrocatalysis for Partial Anionic Substitution in Cobalt Oxysulfide Nanoparticles

Andrew Nelson, Kevin E. Fritz, Shreyas Honrao, Richard G. Hennig, Richard D. Robinson, and Jin Suntivich

Materials

Trioctylphosphine oxide (99%), ammonium sulfide (40-48 wt% solution in water), oleic acid (99%), 1,2-dichlorobenzene (DCB, 99.8%, anhydrous), oleylamine (70%), 1-octadecene (90%), dicobalt octacarbonyl (>90%), Nafion 117 solution (~5% mixture of lower aliphatic alcohols and water), N,N-dimethylformamide (99.8%, anhydrous), pentane (>99%, anhydrous), nitric acid (70%), potassium hydroxide (99.99%), lead (II) nitrate (>99.99%), cobalt (II,III) oxide (nanopowder, 99.5%), 1-butanol (99.8%, anhydrous), and thiourea (>99%) were obtained from Sigma Aldrich and used as received except as noted. The sulfide content of commercially available $(NH4)_2S$ was checked by gravimetric analysis of precipitated lead sulfide formed by adding the sulfide solution to an aqueous solution containing excess $Pb(NO_3)_2$.[1] Oleic acid and DCB were stored under inert atmosphere in a glove box. $Co_2(CO)_8$ was recrystallized from cold pentane immediately before use. Acetylene black (AB, Alfa Aesar, 99.9+%) was treated in nitric acid at 80°C for several hours, then filtered and dried at 100°C overnight. Other chemicals were used as received: isopropyl alcohol (99%) and hexanes (>98.5%) from BDH; cobalt (II) oxide (nanopowder, 99.7%) from US Research Nanomaterials, Inc; ethyl ether (>99%, anhydrous, stabilized with BHT) from Fisher Scientific; cobalt (ii) nitrate hexahydrate (99%) from Acros Organics; and ethanol (200 proof) from KOPTEC. Molecular sieves (Fluka, UOP type 3 A) were activated at 300°C under vacuum for at least 3 hours before use. All aqueous solutions were prepared using 18.2 MΩ water from a Direct-Q system (Millipore).

Nanoparticle Synthesis

CoO nanoparticles were synthesized by oxidation of monodisperse cobalt nanoparticles.[2] Standard Schlenk line techniques were used. In a typical experiment, a three-necked, round-bottom flask was loaded with TOPO (0.1 g), sealed, and purged with nitrogen by three evacuation and backfilling cycles. 12mL of 1,2-dichlorobenzene containing 0.1 mL dissolved oleic acid was added, followed by degassing the solution with three additional evacuation and backfilling cycles. Subsequently, the solution was heated to reflux (180-183°C), and 0.54 g of $Co_2(CO)_8$ dissolved in 3 mL of DCB was quickly injected via syringe. After 10 minutes, growth was stopped by quenching the vessel in a water bath. Ethanol was added (1:1 by volume) to precipitate out the nanoparticles, which were separated by centrifugation, re-suspended in hexane, and precipitated once more with ethanol (2:1 hexane:ethanol) to remove very small particles which remained in the supernatant. The purified nanoparticles were redissolved in DCB; after this solution was heated to 180°C, a gentle stream of air was blown through the solution for 4 hours to quantitatively oxidize the particles to CoO. The particles were then precipitated with ethanol (1:1 DCB:ethanol) followed by centrifugation.

Sulfur-doped cobalt oxides were synthesized by anion exchange according to our previous report.[1] The degree of anion exchange was controlled by varying the amount of added $(NH_4)_2S$. Three different exchange ratios were examined based on the nominal molar ratio of cobalt (assuming particles were

100% CoO) to introduce sulfide: 10:3, 1:1, and 1:3. In a typical experiment, approximately 30mg of CoO nanoparticles were dissolved in 3.5 mL of mixed octadecene and oleylamine (1:1 by volume). This solution, in a sealed three-neck flask, was degassed by three evacuation/backfill cycles with nitrogen on a Schlenk line, then heated to 100°C. A solution of $(NH_4)_2S$ in oleylamine was prepared by dissolving an appropriate amount of aqueous $(NH_4)_2S$ (~56, ~189, or ~589 µL of solution for each ratio above, with an aqueous $(NH_4)_2S$ concentration of 41.7 wt%) in 10 mL of oleylamine followed by drying for about 20 minutes with molecular sieves. 3.5 mL of this solution was injected into the hot solution of CoO_x NPs, after which the temperature was set to 70°C. The color of the solution immediately changed from dark brown to black. The reaction was allowed to proceed for five minutes following injection, then the flask was cooled in a water bath. The anion-exchanged nanoparticles were recovered by precipitation with ethanol/centrifugation and were washed once more by resuspension in hexane followed by precipitation with ethanol/centrifugation.

Annealed NPs were synthesized according to an adaptation of our previous procedure.[1] Approximately 40 mg of NPs of any composition were dissolved in a mixed solvent of 4.4 mL of octadecene and 1.1 mL of ODE in a three-neck flask. After degassing by three evacuation/backfill cycles on a Schlenk line, the solution was heated to 200°C and kept at that temperature for 1 hour, after which it was cooled by removing the heating mantle. The annealed NPs were recovered by precipitation with ethanol/centrifugation and washed once more by resuspension in hexane followed by precipitation with ethanol/centrifugation.

Post-synthetic characterization

Transmission electron microscopy (TEM) and selected area electron diffraction (SAED) images were obtained using an FEI Tecnai T12 at an accelerating voltage of 120 kV. SAED pattern analysis and calibration were done using D.R.G. Mitchell's script for circular Hough transform analysis[3] in Gatan DigitalMicrograph 2.32. Power law background from the forward-scattered beam was subtracted by fitting a portion of the background before the reflections to an equation of the form $y = a \cdot x^b$,[4] and all peaks were fit to Lorentzian distributions. The camera length for each SAED image was calibrated against an evaporated Al foil standard (Electron Microscopy Sciences). The stoichiometry of the products was also checked using an energy-dispersive x-ray spectrometer (EDX) on the same instrument, but without a calibration standard; in general the oxygen content of the samples was found to vary widely from point to point (15-30%) and the S content somewhat less (5-10%).

The ratio of Co:S in a set of nanoparticle samples was quantified using inductively coupled plasma-optical emission spectroscopy (ICP-OES) at the Cornell Geochemistry Laboratory, Cornell University, Ithaca, New York. Samples were digested with hot aqua regia and diluted with a 2% nitric acid matrix for analysis using a Spectroblue ICP-OES spectrometer equipped with an argon torch. Co and S were standardized against concentrations from 2 mg/L to 20 mg/L in 2% nitric acid. Sc was used as an internal standard. Relevant emission lines were: Co, 228.616 nm; S, 180.731 nm; and Sc, 361.384 nm. Relevant operating parameters were: RF power 1450 W, coolant flow 12 L/min, auxiliary flow 0.9 L/min, and nebulizer flow 0.77 L/min.

The particular set of samples shown in **Fig. 1a-d** was found to have the compositions $CoO_{1.6}$, $CoO_{1.6}S_{0.11}$, $CoO_{0.5}S_{0.97}$ and $CoO_{0.5}S_{1.08}$ by EDX. The respective Co:S stoichiometries as found by ICP-OES were CoO_x, $CoO_xS_{0.18}$, $CoO_xS_{1.03}$, and $CoO_xS_{1.27}$. In general this EDX analysis underestimated the amount of S present in the NP samples, especially when the samples were only slightly sulfidized. Given the limitations of

EDX as an analytical technique in this case with less than optimal samples and insufficient calibration,[5] these numbers are of only qualitative importance compared to those found by ICP-OES.

The phase purity of the CoO, Co_3O_4, and CoS_2 nanopowders used as reference materials was checked by x-ray powder diffraction using a Scintag θ-2θ diffractometer with Cu K-alpha radiation. The materials were found to be free of secondary phases (**Fig. S6**).

Catalyst Ink Preparation

Purified particles were dried overnight under vacuum. A 1 mg/mL solution of the nanoparticles in hexane was prepared by re-dispersing the powder using a horn sonicator (Branson Digital Sonifier 450D). A 1 mg/mL solution of AB in N,N-dimethylformamide was prepared similarly. Subsequently, the two immiscible solutions were mixed with the sonicator, causing the carbon to transfer to the hexane phase and uniformly mix with the nanoparticles.

The mixture was precipitated by adding ethanol (1:1 by volume) followed by centrifugation. To remove the long-chain hydrocarbon ligands, the material was re-dispersed with 0.1 M KOH in isopropanol and sonicated for 30 minutes. The catalyst was then precipitated with ethanol, centrifuged, and dried under vacuum overnight, yielding a powder of nanoparticles dispersed on acetylene black.

Electrochemical Testing

Catalyst inks were prepared using isopropanol/water (1:4 by volume) as a solvent; the concentration of catalyst used was 1 mg/mL. Nafion solution was neutralized by addition of 0.1M aqueous KOH (approx. 2:1 KOH:Nafion solutions by volume), then added to the ink (3.4μL per mL) as a binder before mixing by sonication. 10 uL of this catalyst ink, containing 5 μg each of neutralized Nafion, AB, and cobalt oxide/sulfide/oxysulfide nanoparticles was dropcast onto a glassy carbon electrode and allowed to dry under ambient atmosphere. A three-electrode electrochemical cell (Pine) was utilized for all electrochemical measurements and the potential applied to the cell was controlled using a Bio-Logic SP-300 potentiostat. 0.1M KOH was used as the supporting electrolyte. A platinum wire was used as a counter electrode and an Ag/AgCl electrode (Pine) was used as a reference electrode. The potential of this reference electrode was calibrated against the reversible hydrogen electrode (RHE) by measuring the hydrogen evolution/oxidation currents on a polycrystalline Pt disk (Pine) in 0.1M KOH saturated with hydrogen (Airgas, ultra-high purity) and taking the voltage at which the current was zero as 0 V vs. RHE. We measured 0 V vs. RHE to be 0.943 ± 0.005 V vs. Ag/AgCl. All the potentials in this study were referenced to the RHE potential scale and correspond to the applied potentials, $E_{applied,}$ unless they are stated to be iR-corrected potentials, $E_{iR\text{-}corrected}$, calculated with $E_{iR\text{-}corrected} = E_{applied} - iR$ where i is the current and R is the uncompensated ohmic electrolyte resistance. R was taken as the AC impedance at high frequency of the three-electrode system as measured by the same potentiostat.

Cyclic voltammetry measurements were taken by saturating the electrolyte with argon (Airgas, ultra-high purity) prior to measurements and HER measurements were taken after saturating the electrolyte with hydrogen (Airgas, ultra-high purity).

Further remarks on TEM micrographs and SAED structural data

A second population of cobalt oxide NPs was synthesized to produce the annealed $CoO_xS_{0.17}$ sample (**Fig. 2f**, dashed line); which had an as-synthesized diameter of 11.5±1.2 nm immediately after oxidation

(micrograph not shown). Samples of annealed CoO_x and annealed $CoO_xS_{0.17}$, $CoO_xS_{0.88}$, and $CoO_xS_{1.26}$ were all prepared from this population, and they had diameters of 10.8±1.4, 10.1±1.5, 10.5±1.5, and 11.6±1.6 nm respectively (**Fig. S1e-h**).

In the $CoO_xS_{0.88}$ (annealed) sample, one of the phases is consistent with a rocksalt CoO; however, a shift to smaller diffraction angles indicates that the CoO structure is distorted. The second observed phase does not match to either spinel Co_3S_4 or rocksalt Co_9S_8, but matches to Co_9S_8, suggesting the presence of a Co-sulfide phase which is deficient in Co, thus explaining the larger diffraction angles observed. Thus, it appears that there now is sufficient S to form both Co-sulfide domains and substituted oxides. It is unclear whether phase separation occurs within NPs or if they separate into two populations, as we observe that some particles more closely resemble the original oxide particles and some are more similar to the larger, less well-crystallized $CoO_xS_{1.26}$ NPs (see **Fig. S1f**). This observation of phase separation in our annealed oxysulfide NPs may also explain the discrepancy between the observed stoichiometries of the samples reacted at $(NH_4)_2S$:Co ratios 1:1 for the non-annealed ($CoO_xS_{1.03}$) and annealed ($CoO_xS_{0.88}$) samples. The free energies of formation of the individual phases, in particular the stable sulfides (see below), could provide sufficient driving force not only to cause recrystallization of the particles but also to eject excess S under the reducing conditions of the annealing experiment.

The lattice parameter, a, of the cubic unit cell was determined by averaging the lattice parameter found by applying the following equation to the (111), (200), and (220) principal reflections:

$$\frac{1}{d_{hkl}^2} = \frac{h^2 + k^2 + l^2}{a^2} \tag{1}$$

Where d_{hkl} is the interplanar spacing and h, k, and l are the Miller indices. The Debye-Scherrer formula was also used to find the domain size t with a shape factor of 0.9:

$$t = \frac{0.9 \cdot \lambda}{B \cdot \cos\theta_B} \tag{2}$$

λ, the de Broglie wavelength of 120 keV electrons, is 0.0354 Å; B is the full width at half maximum of the Lorentzian fitted peak in radians; and θ_B is the Bragg diffraction angle in radians. No instrumental correction was used. The extracted lattice parameters and crystallite sizes are given in **Table S1**.

Vegard's law calculation

The crystal radii (ionic radii will give an identical result) r_X of 6-fold coordinated Co^{2+} (high spin[6]), S^{2-}, and O^{2-} are taken as 0.885 Å, 1.70 Å, and 1.26 Å respectively, as given by Shannon.[7] Using these radii, the calculated lattice parameter a_{CoO} of rocksalt CoO is 4.29 Å, which compares favorably with the measured value of 4.2612 Å (JCPDS 00-048-1719). We assume that the hypothetical ionic compound CoS has a lattice parameter of 5.17 Å using the Shannon radii. For comparison, ½ of the parameter for Co_9S_8 is 4.9644 Å (JCPDS 00-056-0002). Using Vegard's law to adjust the lattice parameter for the increased radius of S^{2-} to a_{CoOS}:

$$a_{CoOS} = 2 \cdot r_{Co^{2+}} + 2 \cdot X_{CoO} \cdot r_{O^{2-}} + 2 \cdot X_{CoS} \cdot r_{S^{2-}} \tag{3}$$

With the fraction of CoO given by X_{CoO} and of CoS given by X_{CoS}. We find that the lattice parameter should increase by 0.158 Å (relative to the calculated radius of 4.29 Å) assuming perfect substitution of

S^{2-} for O^{2-} in rocksalt CoO for a composition $CoO_{0.82}S_{0.18}$. The deviation found for $CoO_xS_{0.18}$ is +0.021 Å relative to the reference structure, +0.016 Å relative to the un-annealed CoO_x, and +0.027 Å relative to the annealed CoO_x and annealed $CoO_xS_{0.17}$ samples (see above). These deviations are thus nearly an order of magnitude lower than that anticipated by Vegard's law.

Table S1. Structural data extracted from the rotationally averaged SAED patterns of CoO_xS_y nanoparticles given in **Fig. S1**. Measurements are given based on the average of the values fitted from the (111), (200), and (220) CoO rocksalt structure reflections unless noted.

Sample composition	CoO lattice parameter,Å [std. deviation]	CoS_x lattice parameter, Å [std. deviation]	Crystallite size, Å [std. deviation]
CoO_x	4.267 [0.005]		31.2 [2.2]
CoO_x (annealed)	4.256 [0.003]		28.8 [4.4]
$CoO_xS_{0.18}$	4.284 [0.001]		29.2 [4.0]
$CoO_xS_{0.17}$ (annealed)	4.256 [0.003]		30.4 [5.6]
$CoO_xS_{1.03}$	4.309 [0.055]		14.7 [7.3][a]
$CoO_xS_{0.88}$ (annealed)	4.262 [0.031]		24.0 [4.3]
		9.653 [0.180][b]	13.0 [9.0][b]
$CoO_xS_{1.27}$	4.247 [0.063][c]		9.8 [0.2][c]
$CoO_xS_{1.26}$ (annealed)		9.673 [0.160][d]	9.3 [7.7][d]

[a] Crystallite size based on the (111) and (200) reflections. If the much weaker reflection (220) is included, measurement increases to 26.1 (20.5) Å.

[b] Based on the reflections (311) near 2.2 $Å^{-1}$, (511) near 3.3 $Å^{-1}$, and (440) near 3.7 $Å^{-1}$.

[c] Based on the (111) and (200) reflections. Very weak signal.

[d] Based on the reflections (511) near 3.3 $Å^{-1}$ and (440) near 3.7 $Å^{-1}$.

Calculation of the cobalt sulfide content of an oxysulfide NP

In this section, we consider the set of NPs used to generate the annealed sample $CoO_xS_{0.17}$. The average particle size of the cobalt NPs (epsilon phase) used for this sample set as measured by TEM was 9.5 ± 1.2 nm, and the calculated crystallographic density of ε-Co is 8.635 as given by Dinega and Bawendi.[8] Using the average particle size we estimate based on this density that there are on average 39,610 atoms/particle. Assuming this number of Co atoms does not change as the particle is oxidized to CoO and this material is then anion-exchanged with S^{2-}, there are therefore ca. 6,734 S atoms/particle available to form Co-sulfide domains in $CoO_xS_{0.17}$. As there are 32 S atoms in each unit cell (for Co_9S_8 a = 9.9287 Å, Z = 4 per JCPDS 00-056-0002; for Co_3S_4 a = 9.4232 Å, Z = 8 per JCPDS 00-047-1738), enough Co_9S_8 or Co_3S_4 should be formed to produce a single domain of diameter 7.3 nm to 7.0 nm, respectively. Such crystalline domains are not observed in the SAED for $CoO_xS_{0.17}$, indicating that phase segregation is incomplete, likely due to the overall low mobility of S. Where measurable domains of CoS_x *are* observed, their size as measured by the Debye-Scherrer equation is much less than 7 nm (see above, **Table S1**).

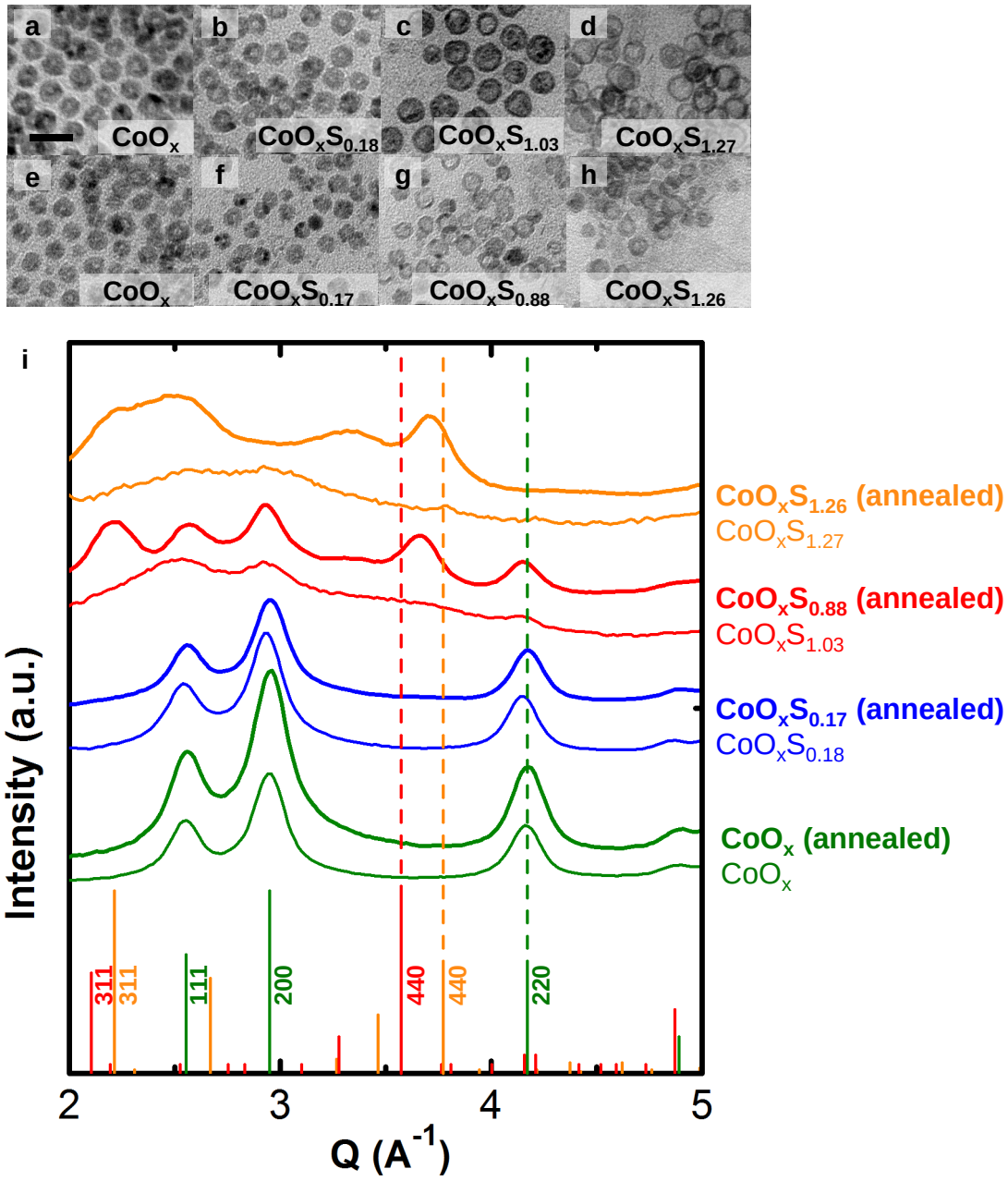

Figure S1. Transmission electron microscopy characterization of structural transformations of CoO_xS_y nanoparticles. Both as-exchanged (a-d, same as Fig. 1a-d) and annealed (e-h) samples are shown. Scale bar is 25 nm. Also shown (i) is an overall summary for the rotationally averaged SAED patterns of the the NPs, with reflections from rocksalt CoO (brown, JCPDS 00-048-1719), rocksalt Co_9S_8 (red, JCPDS 00-056-0002), and spinel Co_3S_4 (green, JCPDS 00-047-1738) indicated; prominent lines are indicated with their Miller indices. Dashed lines are drawn for key reflections as a guide to the eye.

Calculation of the catalyst active area

Particle and void diameters $d_{particle}$ and d_{void} were measured from TEM images using at least 250 measurements. From these measurements the geometric surface area of each particle A_s was calculated assuming that only the outer surface contributed to the area:

$$A_s \approx \frac{\sum 4 \cdot \pi \cdot r_{particle}^2}{\sum \left(\frac{4}{3}\right) \cdot \rho \cdot \pi \cdot \left(r_{particle}^3 - r_{void}^3\right)} = \frac{6}{\rho} \cdot \frac{\sum d_{particle}^2}{\sum \left(d_{particle}^3 - d_{void}^3\right)} \quad (4)$$

Because the material density ρ is not known with certainty, it was estimated by taking a weighted average of bulk densities. For the catalysts based on CoO_x, $CoO_xS_{0.18}$, and $CoO_xS_{0.17}$, which are all isostructural, the weighted average of the densities of cobalt (ii) oxide[9] (6.44 g/cm^3) and cobalt (ii) sulfide[9] (5.45 g/cm^3) were used based on the hypothetical compound $CoO_{1-y}S_y$, where y is the measured S:Co ratio. For the amorphized catalysts $CoO_xS_{1.03}$ and $CoO_xS_{1.27}$, the density was estimated by taking a weighted average of the bulk densities of CoO and Co_3S_4 (4.843 g/cm^3, JCPDS 00-047-1738) based on the hypothetical compound $(CoO)_{1-3y/4}(Co_3S_4)_{3y/4}$, again where y is s equal to the measured S:Co ratio.

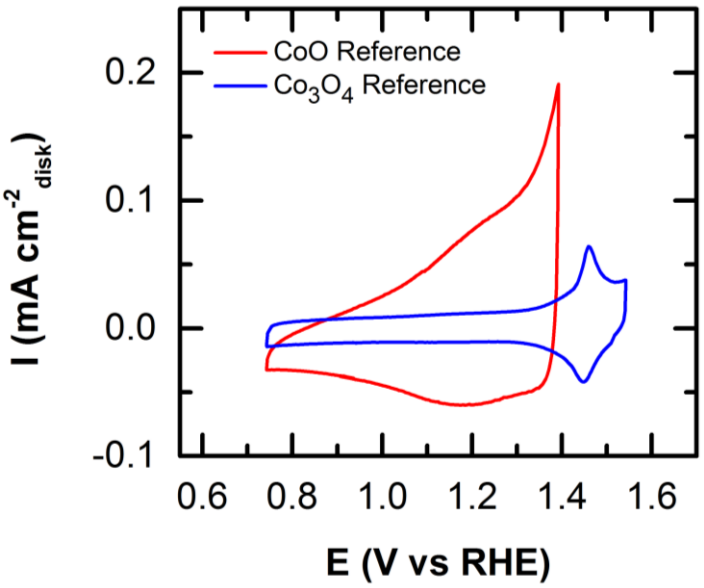

Figure S2. Cyclic voltammograms of carbon-supported thin-film electrocatalysts containing CoO (red line) and Co_3O_4 (blue line) nanopowders in Ar-saturated 0.1 M KOH at 50 mV/s scan rate.

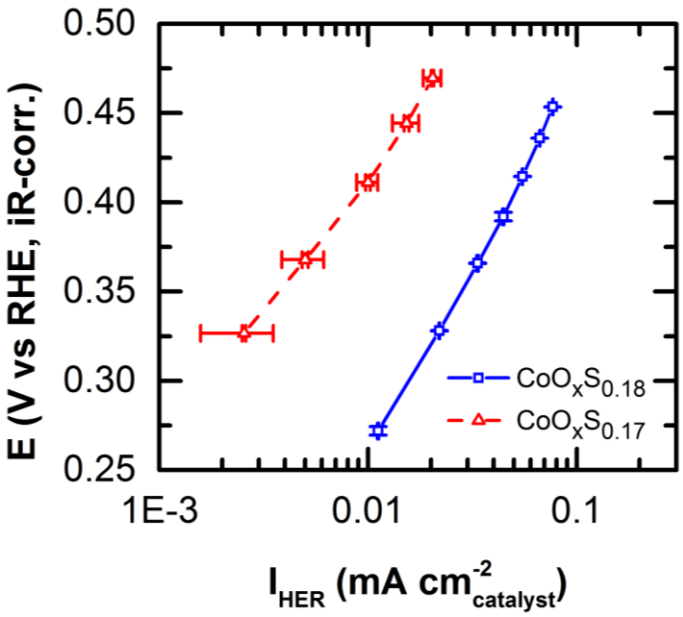

Figure S3. Tafel plot comparing un-annealed $CoO_xS_{0.18}$ (blue curve) with annealed $CoO_xS_{0.17}$ (red curve) is shown based on the known geometries of the particles. It is seen that the activity of the annealed catalyst at 375 mV vs. RHE is lower than that of the un-annealed one by nearly an order of magnitude. Error bars give the standard deviation from three independent measurements.

Density Functional Theory Calculations

Density-functional theory (DFT) calculations were performed with the Vienna Ab-initio Software Package (VASP)[10-13] using the PBE exchange-correlation functional[14] and the projector augmented wave method.[15, 16] The Brillouin zone integration was performed using a Monkhorst and Pack *k*-point mesh.[17] 3×3×1 *k*-point meshes were employed for structural relaxations and energy calculations for the slabs. The energy cutoff for the plane wave basis was set to 400 eV and the corresponding cutoff energies for the augmentation functions were set to 650 eV for all our calculations. We did not employ the DFT+U method here for the reason that the results depend sensitively on the Hubbard U value. Furthermore, it is expected that U should depend on the local environment of the Co atoms, resulting in a different value required in the bulk, on the surface, and as a function of the S composition. To avoid this complication and resulting arbitrariness, we performed our calculations of the H adsorption energies on the S substituted CoO surfaces using the PBE approximation.

We used a 64-atom CoO(100) slab to calculate the adsorption and formation energies, since CoO is the most stable Co oxide phase under our experimental conditions; furthermore, the (100) surface is used because it has the lowest energy and is charge neutral. A vacuum spacing of 12 Å was used to ensure that the surface does not interact with its periodic image. Only the top two layers of the slab are allowed to relax. We first determine whether a substitutional S atom prefers to sit on a surface site or in the bulk. For just a single S, it was 0.65 eV more expensive for S to replace a surface O atom compared to one sitting in the second layer. However, as we added more S atoms, the energy required to sit on the bulk site started going up; the surface was now a better site for these S atoms. We attribute this

increase in energy to the fact that the S anion is considerably larger than the O anion, starting to cause strain inside the slab. Furthermore, the migration barrier for S to diffuse into the CoO slab is quite high at 2.63 eV, preventing inward diffusion.[1] This supports our conclusion that most of the sulfur in our experiment must be present on the surface.

Our formation energy calculations combined with the Co-O-S phase diagram from the Materials Project website[18, 19] suggest that a mixture of cobalt oxides and sulfides will be lower in energy than the rocksalt CoO_xS_y phase. Based on calculated energies for bulk CoO and Co_3S_4 phase, we estimate that the rocksalt CoO_xS_y structure with all surface O atoms replaced by S would be at least 0.17 eV/atom more unstable than a phase separated mixture of CoO and Co_3S_4.

We calculated the adsorption energies of H* for the same size slab. Starting with the pure CoO slab, we successively replaced O atoms on the surface with S until all the surface anion sites (8) were occupied by S. Placing a single H atom on top of Co, O and S sites, we calculated adsorption energies for each case. All possible configurations of the surface were considered, and we picked the one with the lowest energy as it indicates strongest binding. Reference values for H-adsorption energy on platinum were obtained using a 64-atom Pt (111) slab. A schematic of the CoO slab is shown in **Fig. S4**. The results are shown in **Fig. S5**; the results of every calculation are shown in **Table S2**.

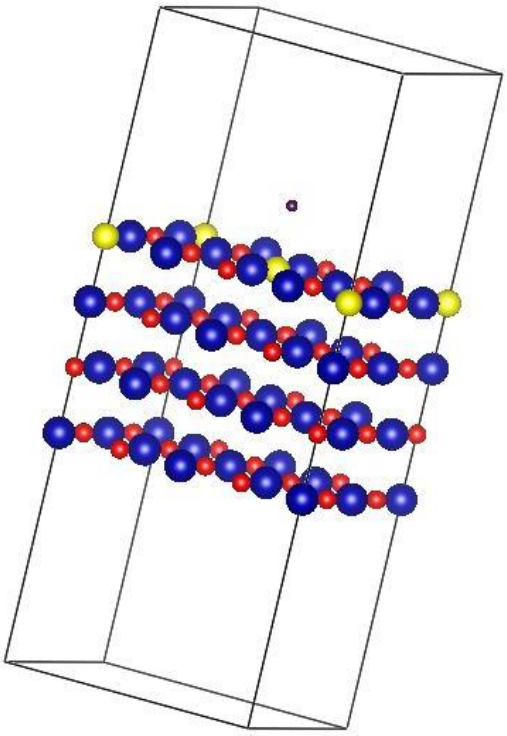

Figure S4. DFT structural model showing the 2x2 unit cell CoO(100) slab (c-direction). Red: Co atoms; blue: O atoms; yellow: S atoms. Small red atom is an H atom.

Table S2. Results of the DFT calculations for the binding energy of H. **Bold** numbers indicate that the energy is the minimum calculated for the species that H sits on for each S substitution.

# of S on surface	Location of H	Species H sits on	Defect Formation Energy (eV)
0	edge	Co	**0.49**
0	center	O	**1.23**
1	edge	Co	1.03
1	inside	Co	**-0.29**
1	corner	O	6.38
1	octahedral	O	5.63
1	tetrahedral	O	**1.97**
1	center	S	**6.23**
2	inside	Co	-0.14
2	edge	Co	**-0.15**
2	tetrahedral	O	2.22
2	octahedral	O	**2.21**
2	center	S	1.97
2	corner	S	**1.90**
3	edge	Co	0.48
3	inside	Co	**0.20**
3	tetrahedral	O	2.71
3	corner	O	**2.13**
3	octahedral	S	1.78
3	center	S	**1.43**
4	edge	Co	**0.43**
4	inside	Co	**0.43**
4	tetrahedral	O	**1.64**
4	corner	S	2.36
4	center	S	1.55
4	octahedral	S	**1.27**
8	edge	Co	**0.65**
8	center	S	**0.78**

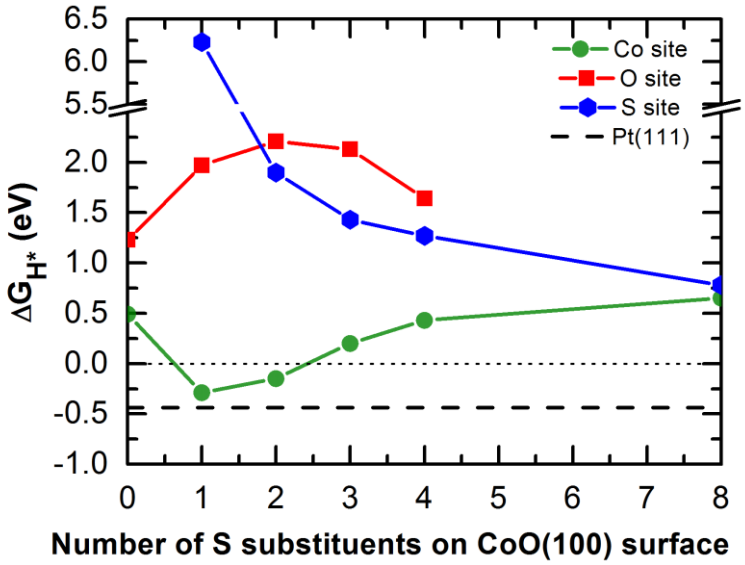

Figure S5. Results from the DFT calculation of binding energies of H* to various sites on the (modified) CoO(100) surface. Adsorption of H is always favored on Co; only at very high levels of S substitution at the surface does binding to S become comparatively favorable. At only 1 anion site in 8 replaced with S, the adsorption energy approaches that of the highly active Pt(111).

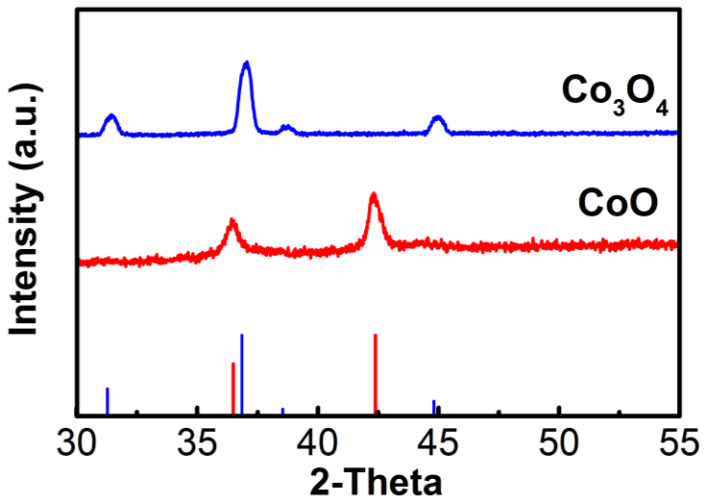

Figure S6. XRD patterns for Co_3O_4 (JCPDS 00-042-1467, blue line) and CoO (JCPDS 00-048-1719, red line) nanopowder reference samples.

CoS_2 Nanoparticle Electrochemical Testing

We use cobalt disulfide as a reference HER activity for an active sulfide-rich cobalt disulfide phase.[20] , We synthesized phase-pure CoS_2 nanopowder via the thermal decomposition of $Co[SC(NH_2)_2]_4(NO_3)_2$ at 400 °C under N_2 for 2 h, as described previously.[21] The CoS_2 phase was confirmed with XRD (**Fig. S7**, left) and the particle size was characterized with TEM (**Fig. S7**, right), shown below. Based on TEM analysis, the particle size is 13.0 nm ± 4.3 nm, in agreement with the crystallite size extracted from XRD using the Scherrer equation (13.7 ± 1.5 nm, from 8 strongest reflections).

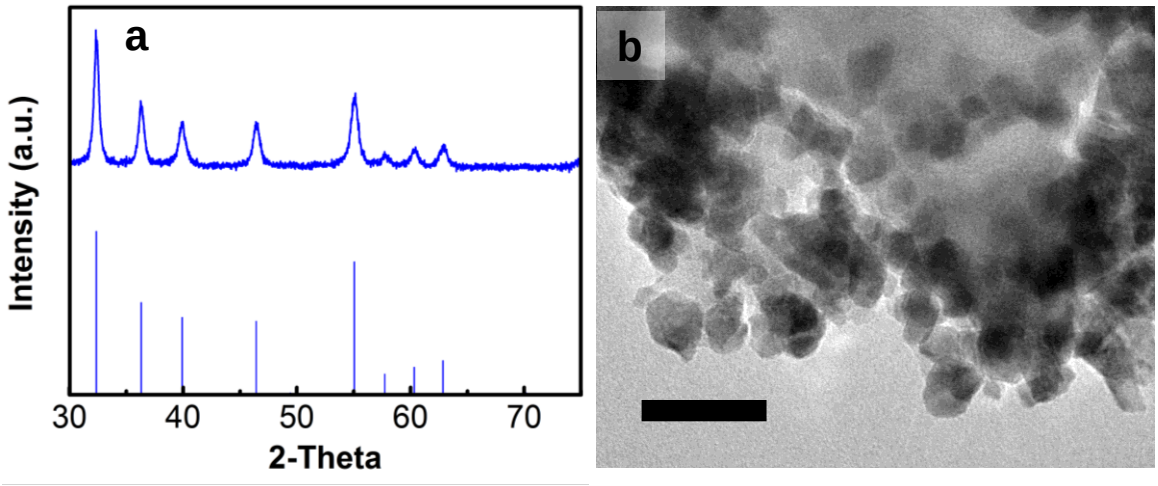

Figure S7. Structure and morphology of CoS_2 nanoparticles, as characterized by XRD (a) and TEM (b). All peaks can be indexed to the CoS_2 structure (JCPDS 01-070-2865). Scale bar is 50 nm.

We characterize the HER activity of the CoS_2 nanoparticles using the same electrode protocol that was used to characterize the Co oxysulfide. We find that CoS_2 has a lower specific activity and mass activity than CoO_x as well as $CoO_xS_{0.18}$, as seen in the Tafel plots below (**Fig. S8**). Further, the CoS_2 showed significant activity degradation after only five cycles. Therefore, we can conclude on the basis of this preliminary characterization that the improved activity seen in the mixed anion compounds does not result from a possible sulfide-rich CoS_2-like phase on the Co-oxysulfide surface.

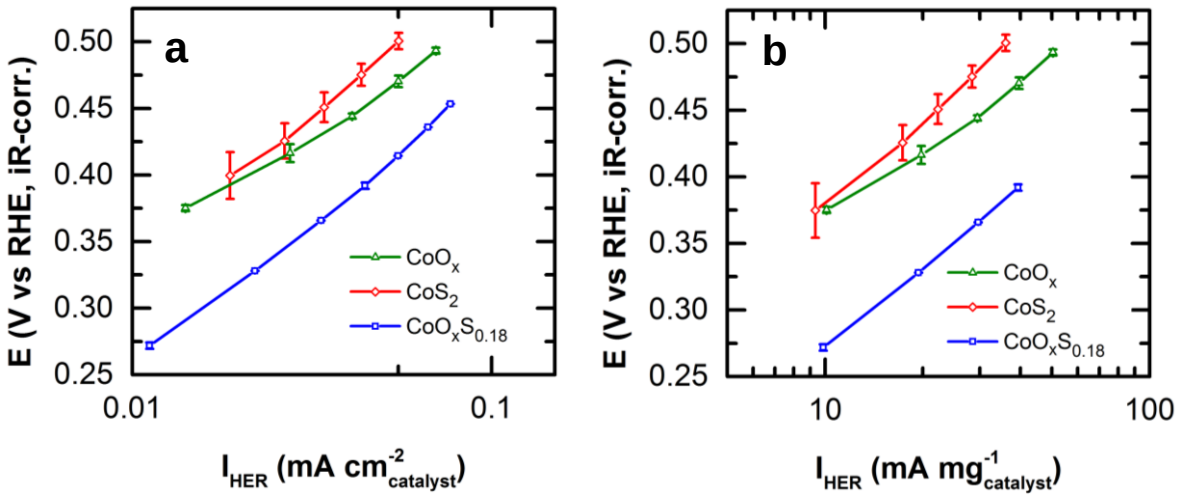

Figure S8. Tafel plots of the (a) specific activities and (b) mass activities of cobalt oxide (CoO_x), oxysulfide ($CoO_xS_{0.18}$) and sulfide (CoS_2). The activity of CoS_2 is ~4x lower than that of the Co oxysulfide.

References

1. H. Zhang, L. V. Solomon, D.-H. Ha, S. Honrao, R. G. Hennig and R. D. Robinson, *Dalton Transactions*, 2013, **42**, 12596-12599.
2. Y. Yin, R. M. Rioux, C. K. Erdonmez, S. Hughes, G. A. Somorjai and A. P. Alivisatos, *Science*, 2004, **304**, 711-714.
3. D. R. G. Mitchell, *Ultramicroscopy*, 2008, **108**, 367-374.
4. Z. Luo, Y. Vasquez, J. F. Bondi and R. E. Schaak, *Ultramicroscopy*, 2011, **111**, 1295-1304.
5. D. B. Williams and C. B. Carter, *Transmission Electron Microscopy: A Textbook for Materials Science*, Springer-Verlag, 2009.
6. J. B. Goodenough, *Physical Review*, 1960, **117**, 1442-1451.
7. R. D. Shannon, *Acta Crystallographica*, 1976, **A32**, 751-767.
8. D. P. Dinega and M. G. Bawendi, *Angewandte Chemie International Edition*, 1999, **38**, 1788-1791.
9. W. M. Haynes, T. J. Bruno and D. R. Lide, eds., *CRC Handbook of Chemistry and Physics, 96th edition*, CRC Press, Boca Raton, FL, 2015.
10. G. Kresse and J. Furthmüller, *Physical Review B*, 1996, **54**, 11169.
11. G. Kresse and J. Furthmüller, *Computational Materials Science*, 1996, **6**, 15-50.
12. G. Kresse and J. Hafner, *Physical Review B*, 1994, **49**, 14251.
13. G. Kresse and J. Hafner, *Physical Review B*, 1993, **47**, 558.
14. J. P. Perdew, K. Burke and M. Enzerhof, *Physical Review Letters*, 1996, **77**, 3865.
15. P. E. Blöchl, *Physical Review B*, 1994, **50**, 17953.
16. G. Kresse and D. Joubert, *Physical Review B*, 1999, **59**, 1758.
17. H. J. Monkhorst and J. D. Pack, *Physical Review B*, 1976, **13**, 5188.
18. A. Jain, S. P. Ong, G. Hautier, W. Chen, W. D. Richards, S. Dacek, S. Cholia, D. Gunter, D. Skinner, G. Ceder and K. A. Persson, *APL Materials*, 2013, **1**, 011002.
19. A. Jain, G. Hautier, S. P. Ong, C. J. Moore, C. C. Fischer, K. A. Persson and G. Ceder, *Physical Review B*, 2011, **84**, 045115.
20. M. S. Faber, M. A. Lukowski, Q. Ding, N. S. Kaiser and S. Jin, *The Journal of Physical Chemistry C* 2014, **118**, 21347-21356.

21. N. Kumar, N. Raman and A. Sundaresan, *Zeitschrift für anorganische und allgemeine Chemie*, 2014, **640**, 1069-1074.